Determination of the aerodynamic droplet breakup boundaries based on a total force approach

George Strotos[a,1,*], Ilias Malgarinos[b,c,2], Nikos Nikolopoulos[c,3], Manolis Gavaises[b,4], Konstantinos-Stephen Nikas[d,5], Kostas Moustris[d,6]

[a]Technological Educational Institute of Thessaly, Mechanical Engineering Department, 41110 Larissa, Greece

[b]School of Engineering and Mathematical Sciences, City University London, Northampton Square, EC1V 0HB, London, UK

[c]Centre for Research and Technology Hellas/Chemical Process and Energy Resources Institute (CERTH/CPERI), Egialeias 52, Marousi, Greece

[d]Piraeus University of Applied Sciences, Mechanical Engineering Department, 250 Thivon and P. Ralli str., Aegaleo 12244, Greece

[1] gstrot@teilar.gr

[2] Ilias.Malgarinos.1@city.ac.uk , malgarinos@lignite.gr

[3] n.nikolopoulos@certh.gr

[4] M.Gavaises@city.ac.uk

[5] ksnikas@puas.gr

[6] kmoustris@puas.gr

[*]Corresponding author

Abstract

The determination of the critical We_g number separating the different breakup regimes has been extensively studied in several experimental and numerical works, while empirical and semi-analytical approaches have been proposed to relate the critical We_g number with the Oh_l number. Nevertheless, under certain conditions, the Re_g number and the density ratio ε may become important. The present work provides a simple but reliable enough methodology to determine the critical We_g number as a function of the aforementioned parameters in an effort to fill this gap in knowledge. It considers the main forces acting on the droplet (aerodynamic, surface tension and viscous) and provides a general criterion for breakup to occur but also for the transition among the different breakup regimes. In this light, the present work proposes the introduction of a new set of parameters named as $We_{g,eff}$ and Ca_l monitored in a new breakup plane. This plane provides a direct relation between gas inertia and liquid viscosity forces, while the secondary effects of Re_g number and density ratio have been embedded inside the effective We_g number ($We_{g,eff}$)

Keywords: droplet breakup; critical *We* number; VOF simulations

1 Introduction

The aerodynamic droplet breakup has been extensively studied in experimental and numerical works due to its importance in spray systems. Depending on the relative strength of the main forces acting on the droplet (aerodynamic, surface tension and viscous forces), different breakup types can be observed such as the bag breakup, the transitional breakup (including several sub-types), the sheet-thinning breakup and the catastrophic breakup. A complete description of these breakup modes can be found in the review article of (Guildenbecher et al., 2009) among others.

Increasing the gas phase inertia results in the successive transition between the aforementioned breakup regimes. The parameters affecting droplet breakup are grouped into dimensionless numbers, such as the We_g, the Oh_l and the Re_g numbers, but also the density and viscosity ratios of the liquid/gas phase (ε and N respectively); see section 2.1 for a complete description of these numbers. Among them, the We_g number is the most influential, while the liquid viscous damping becomes important only when Oh_l>0.1; see for example the breakup map of (Hsiang and Faeth, 1995).

The We_g number leading to droplet breakup (or generally separating different breakup regimes) is called critical *We* number ($We_{g,cr}$) and in the limit of negligible liquid viscosity (i.e. low Oh_l), we call it in the present work as $We_{g,cr,0}$ (the subscript 0 denotes negligible viscosity). Having also in mind that the experimental data are characterized by high Re_g numbers, the $We_{g,cr,0}$ generally represents negligible viscosity effects both in the gas and liquid phases. In the following paragraphs, the various approaches found in literature to relate $We_{g,cr}$ with $We_{g,cr,0}$ will be presented.

In (Guildenbecher et al., 2009) it is stated that breakup is observed for $We_{g,cr,0}$=11±2, indicating that there is a scatter in the results of experimental works; in (Hanson et al., 1963) an even lower value of ~7 is reported. Regarding the dependency between the $We_{g,cr}$ and Oh_l numbers (the two most influential), this is generally expressed through the empirical equation 1, where *C* and *n* are fitting coefficients:

$$\frac{We_{g,cr}}{We_{g,cr,0}} = 1 + C \cdot Oh_l^n \tag{1}$$

A list of the coefficients *C*, *n* which were determined in past works is given in Table 1. (Brodkey, 1967) and (Gelfand, 1996) obtained these coefficients by fitting experimental data, while (Cohen, 1994) assumed that the energy required for breakup, is that of an inviscid droplet plus the energy required to overcome the viscous dissipation (see details in section 6.3); this resulted in *n*=1, while the coefficient *C* was determined by fitting experimental data.

Table 1: List of the coefficients *C*, *n* of eq. 1 proposed by different sources for the bag breakup regime.

source	**coeff. *C***	**coeff. *n***	**derivation**	**comments**
(Brodkey, 1967)	1.077	1.6	Empir.	Oh_l<10
(Cohen, 1994)	1-1.8	1	Semi-Anal.	10<$We_{g,cr,0}$<100
(Gelfand, 1996)	1.5	0.74	Empir.	Oh_l<4

In (Hsiang and Faeth, 1995) the droplet momentum equation was used and adopting the viscous timescale of (Hinze, 1949) (eq. 14 in section 2.1), they derived equation 2. Assuming an average value of the drag coefficient $\overline{C_D}$, they determined the coefficient *C* (without mentioning its value) by comparing against experimental data and the model performance was very good.

$$\frac{We_{g,cr}}{We_{g,cr,0}} = \frac{1}{4}\left(1 + C \cdot \frac{\overline{C_D}}{\sqrt{\varepsilon \cdot We_{g,cr,0}}} Oh_l\right)^2 \quad (2)$$

Another approach for the estimation of the critical We_g number, is to assume that the breakup is ought to Rayleigh-Taylor (R-T) instabilities as in (Zhao et al., 2011) and (Yang et al., 2017). According to this model, when the droplet deformation (usually the cross-stream diameter) exceeds the critical wavelength of the R-T instability (which depends on liquid properties and droplet acceleration), then breakup occurs. The resulting equation (e.g. in (Zhao et al., 2011)) has the form of eq. 3, where *C* is an adjustable coefficient, in the range 1.18-1.48.

$$\left(\frac{We_{g,cr,0}}{We_{g,cr}}\right)^{1/2} + C\left(\frac{Oh_l^2}{We_{g,cr}}\right)^{1/3} = 1 \quad (3)$$

The concept of R-T instabilities has been considered as the main mechanism for breakup in other works as in (Joseph et al., 1999),(Theofanous and Li, 2008), (Theofanous et al., 2012). The group of Prof. Theofanous considered also a different characterization of breakup, with Rayleigh-Taylor piercing (RTP) happening at lower We_g numbers and shear-induced entrainment (SIE) above a transition We_g. Generally,

the aforementioned correlations are in qualitative agreement between them, but they do not give insight into the effects of Re_g and ε numbers

Turning now to the effect of the Re_g number and density ratio ε, this has not been in detail examined in experimental works due to technical limitations in obtaining low Re_g and ε numbers. On the other hand, their effect has been examined in a few numerical works but without providing correlations similar to the aforementioned for the Oh_l number (e.g. as in eq. 1). As a general remark, they have all concluded that the critical We_g number increases for low Re_g and ε numbers. More specifically, (Aalburg, 2002) found that there is no effect on breakup for Re_g>100 and ε>32. Nevertheless, their numerical model could not predict the actual breakup and they assumed that breakup happens when the cross-stream deformation exceeds 60%; despite this limitation, they were able to reproduce the breakup map of (Hsiang and Faeth, 1995). In (Han and Tryggvason, 2001) the authors examined low density ratios (ε<10) and found that the Re_g effect is minimal for Re_g>200, while decreasing the Re_g and keeping the other parameters constant can lead to different breakup modes. A similar conclusion was also drawn when the density ratio decreases and approaches unity. In (Jing and Xu, 2010) it is stated that shear breakup is observed only for ε>100, while for Re_g numbers in the range 10^2 up to 10^6 there are slight differences in the topology of the bag and the rim. Regarding the effect of density ratio they found different breakup modes for ε=10 and 1000 (forward bag and sheet-thinning respectively for We_g=27.5) and also significantly lower droplet acceleration and displacement as the density ratio increases. Recently, (Yang et al., 2016) used a 3D model to study breakup at highly unstable conditions (Re_g~10^4) and found that breakup is affected even for ε>32 (the limit proposed by (Aalburg, 2002)), and a

lower density ratio results in a higher deformation rate but less intensive fragmentation. Finally, (Kékesi et al., 2014) examined various combinations of Re_g and ε numbers (generally low values) and identified new breakup regimes that have not been observed in experiments.

The aim of the present work is to provide a simple but reliable methodology to relate the critical We_g number with all the actual dimensionless numbers affecting droplet breakup, as there is a lack of such a model in literature. In the text follows there is a description of the methodology and then the model results are presented. In the appendix, the derivation of correction factors for the effect of Re_g number and density ratio is presented along with a correlation to predict the breakup initiation time. Finally in the appendix, the present methodology is related to a modified version of the energy approach of (Cohen, 1994), showing that both concepts are equivalent.

2 Methodology

2.1 Forces and dimensionless numbers

Before proceeding to the presentation of the methodology adopted in the present work, it is essential to discuss the forces acting on the droplet and the dimensionless numbers describing droplet breakup.

The main forces controlling droplet breakup are the aerodynamic forces induced from the gas phase ($\sim\rho_g U_g^2 D^2$), the surface tension forces ($\sim\sigma D$), the gas viscosity forces ($\sim\mu_g \mathrm{U}_g D$) and the liquid viscosity forces ($\sim\mu_l \mathrm{U}_l D$). In the latter case, the liquid

velocity U_l appearing can be estimated from (Hinze, 1955), (Hsiang and Faeth, 1992) as:

$$U_l = \sqrt{\frac{\tau}{\rho_l}} = \sqrt{\frac{\rho_g U_g^2}{\rho_l}} = \frac{U_g}{\sqrt{\varepsilon}} \tag{4}$$

, where $\varepsilon = \rho_l/\rho_g$ is the density ratio and τ denotes stress. This equation implies that gas and liquid inertia forces are essentially equal to one another ($\rho_l U_l^2 = \rho_g U_g^2$). Turning now to the definition of the dimensionless numbers, these are derived by combing different types of forces:

$$We_g \sim \frac{gas\ inertia\ forces}{surface\ tension\ forces} = \frac{\rho_g U_g^2 D^2}{\sigma D} = \frac{\rho_g U_g^2 D}{\sigma} \tag{5}$$

$$Oh_l \sim \frac{liquid\ viscous\ forces}{\sqrt{(inertia\ \cdot\ surface\ tension)\ forces}} = \frac{\mu_l \mathrm{U}_l D}{\sqrt{\rho_l U_l^2 D^2 \cdot \sigma D}} = \frac{\mu_l}{\sqrt{\sigma D \rho_l}} \tag{6}$$

$$Re_g \sim \frac{gas\ inertia\ forces}{gas\ viscous\ forces} = \frac{\rho_g U_g^2 D^2}{\mu_g \mathrm{U}_g D} = \frac{\rho_g \mathrm{U}_g D}{\mu_g} \tag{7}$$

Among them, the We_g and the Oh_l numbers are the most influential in droplet breakup, while one can notice that the Oh_l number despite its wide use and importance, it has a rather strange physical meaning by relating the liquid viscous forces with the square root of inertia times surface tension forces.

Using different combinations of the aforementioned forces, one can define additional dimensionless numbers, such as the liquid and gas Capillary numbers (Ca_l and Ca_g), the liquid *Re* number (Re_l) and the gas-liquid *Re* number ($Re_{g/l}$):

$$Ca_l \sim \frac{liquid\ viscous\ forces}{surface\ tension\ forces} = \frac{\mu_l \mathrm{U}_l D}{\sigma D} = \frac{\mu_l \mathrm{U}_g}{\sigma\sqrt{\varepsilon}} \quad (8)$$

$$Ca_g \sim \frac{gas\ viscous\ forces}{surface\ tension\ forces} = \frac{\mu_g \mathrm{U}_g D}{\sigma D} = \frac{\mu_g \mathrm{U}_g}{\sigma} \quad (9)$$

$$Re_l \sim \frac{liquid\ inertia\ forces}{liquid\ viscous\ forces} = \frac{\rho_l U_l^2 D^2}{\mu_l \mathrm{U}_l D} = \frac{\rho_l U_g\ \mathrm{D}}{\mu_l\sqrt{\varepsilon}} = Re_g \frac{\sqrt{\varepsilon}}{N} = \frac{\sqrt{We_g}}{Oh_l} \quad (10)$$

$$Re_{g/l} \sim \frac{gas\ inertia\ forces}{liquid\ viscous\ forces} = \frac{\rho_g U_g^2 D^2}{\mu_l \mathrm{U}_l D} = \frac{\sqrt{\rho_g \rho_l} U_g\ \mathrm{D}}{\mu_l} = Re_g \frac{\sqrt{\varepsilon}}{N} \quad (11)$$

The gas-liquid *Re* number ($Re_{g/l}$) and the liquid *Re* number (Re_l) is proved to represent the same quantity. Both of them are equal to $Re_g\sqrt{\varepsilon}/N$ or $\sqrt{We_g}/Oh_l$; the latter was used in (Aalburg, 2002) to develop a new breakup map as it was proved to dominate the breakup at large Oh_l numbers. The gas-liquid *Re* number ($Re_{g/l}$) has also appeared in the work of (Schmehl, 2002), named there as "deformation" *Re* number. Finally, the term $N/\sqrt{\varepsilon}$ in equations 10 and 11 depends on the physical properties and has appeared in (Gelfand, 1996), (Aalburg, 2002), while in (Kékesi et al., 2014) it was also used to develop a new breakup map along with the Re_g number. Among the aforementioned new dimensionless numbers, the Ca_l number will be proved in the subsequent sections to be the most valuable one and it is related to the other numbers with the following equation:

$$Ca_l = \frac{\mu_l \mathrm{U}_g}{\sigma\sqrt{\varepsilon}} = Oh_l\sqrt{We_g} = \frac{We_g}{Re_l} \quad (12)$$

Finally, for the non-dimensionalization of time, the shear breakup timescale of (Nicholls and Ranger, 1969) is widely used (eq. 13), which in fact represents the liquid convection timescale. For large Oh_l numbers, the viscous timescale of (Hinze, 1949) has also been used (eq. 14)

$$t_{sh} = \frac{D}{U_l} = \frac{D\sqrt{\varepsilon}}{U_g} \tag{13}$$

$$t_{vis} = \frac{\mu_l}{\rho_g U_g^2} = t_{sh}/Re_l \tag{14}$$

2.2 Total Force approach

As mentioned in the previous section 2.1, there are various types of forces acting on the droplet. One can group them into forces that tend to deform the droplet (F_{DEF}) and forces tending to restore the droplet (F_{RES}) in its original shape, or equivalently into forces from the gas side (F_{gas}) and forces from the liquid side (F_{liq}). These two types of forces are overall calculated as in equations 15 and 16,

$$F_{DEF/gas} = \rho_g U_g^2 D^2 - C_{vis,g}\mu_g U_g D \tag{15}$$

$$F_{RES/liq} = \sigma D + C_{vis,l}\mu_l U_l D \tag{16}$$

, where the terms $C_{vis,g}$ and $C_{vis,l}$ are adjustment factors aiming to reveal the contribution of the gas and liquid viscous forces correspondingly on the evolution of the phenomenon. For convenience here, the gas viscous forces (which are restorative) appear in the deformation forces but with a negative sign. Thus, the term $F_{DEF/gas}$ represents the net deformation forces from the gas side.

The ratio of these forces is called here *TFR* (Total Force Ratio) and it is shown in eq. 17, in which the liquid velocity U_l has been replaced with the corresponding gas terms according to eq. 4:

$$TFR = \frac{F_{DEF/gas}}{F_{RES/liq}} = \frac{\rho_g U_g^2 D^2 - C_{vis,g}\mu_g U_g D}{\sigma D + C_{vis,l}\mu_l \frac{U_g}{\sqrt{\varepsilon}} D} \quad (17)$$

Diving both forces with σD (the surface tension forces) and after some manipulation of eq. 17 we can reach the following equation 18, where $f_{vis,g}$ represents a correction factor for the gas viscosity effects.

$$TFR = \frac{We_g}{f_{vis,g}\left(1 + C_{vis,l} \cdot Ca_l\right)} \quad (18)$$

$$f_{vis,g} = \frac{1}{1 - C_{vis,g}\left(1/Re_g\right)} \quad (19)$$

As seen, the *TFR* is in fact the We_g number divided/corrected by two terms (both higher than unity) to account for viscosity effects. In the limit of inviscid flow, *TFR* is simply the We_g number and a close physical approximation of this situation corresponds to conditions characterized by low Oh_l and high Re_g numbers.

The model proposed in this study, assumes that there is a critical *TFR* value (TFR_{cr}), above which, breakup occurs (or there is generally transition among the different breakup modes). It is further assumed that the critical *TFR* value depends only on the breakup mode (bag, sheet-thinning etc) and not on other dimensionless numbers (e.g. the Oh_l number as in the case of $We_{g,cr}$), since by definition *TFR* accounts for all types

of forces. This critical value pertains to the $We_{g,cr,0}$ value, which depends only on the breakup mode and it is generally known from experiments ($We_{g,cr,0}$ was defined in the introduction for low Oh_l and high Re_g numbers).

Nevertheless, there is also one parameter that has not been yet included in the present analysis. This is the density ratio ε. Past works (presented in the introduction) have shown that the critical We_g number increases for low ε values, thus the $We_{g,cr,0}$ has to be multiplied by a correction factor $f\varepsilon$ ($f\varepsilon$>1) to account for low density ratio effects. Thus the final criterion for breakup should be defined as $TFR_{cr}=We_{g,cr,0} \cdot f_{\varepsilon}$.

Replacing the TFR_{cr} from eq. 18, the following equations 20-23 describe the relation among $We_{g,cr}$ and the rest dimensionless numbers.

$$\frac{We_{g,cr}}{We_{g,cr,0}} = f_{\varepsilon} \cdot f_{vis,g} \cdot f_{vis,l} \tag{20}$$

$$f_{\varepsilon} = 1 + C_{\varepsilon}\frac{1}{\varepsilon} \tag{21}$$

$$f_{vis,g} = \frac{1}{1 - C_{vis,g}\left(Re_g\right)^{-ng}} \tag{22}$$

$$f_{vis,l} = 1 + C_{vis,l} \cdot (Ca_l)^{nl} \tag{23}$$

The density correction factor $f\varepsilon$ is given by equation 21 with C_{ε}=3 (see section 6.1.2 for details), while the gas and liquid viscosity correction factors are re-written in equations 22 and 23 in a more generic way (using the exponents *ng*, *nl*) to account for deviations from the preceding theoretic analysis (theoretically it is *ng*=*nl*=1).

Regarding the adjustable coefficients $C_{vis,g}$ and ng for the effect of gas viscosity in eq. 22, these were determined by performing numerical simulations (see section 6.1.1 for details) and found to be equal to $C_{vis,g}$=55 and ng=1.1, following a best fitting algorithm, which is close to the estimated value of 1. Regarding the liquid viscosity coefficients, these were depending on the breakup mode and were estimated to be in the range $C_{vis,l}$=0.06 – 0.26 and nl=0.9 – 1.0 (close to the theoretic value of 1); nevertheless, a value of nl=1 was used throughout this study for all breakup modes. These were initially determined based on the breakup boundaries of (Hsiang and Faeth, 1995) and then fine-tuned using the experimental and numerical data shown in sections 3.2.2 and 3.2.3.

The values used for the adjustable coefficients $C_{vis,g}$, $C_{vis,l}$, ng, nl and C_{ε} are given in Table 2, as well as the $We_{g,cr,0}$ value; the catastrophic breakup regime is also included, but it has been estimated without having a sufficient amount of data. All these coefficients are assumed, for the current status of work, to be constant numbers but it is likely, that they are functions of additional numbers (e.g the density ratio), or there are interdependencies between them. It has also to be noted, that all coefficients were assumed to be unaffected by the breakup mode, except of the $C_{vis,l}$ coefficient which is the most influential.

Table 2: Values of the adjustable coefficients $C_{vis,g}$, ng, $C_{vis,l}$, nl, C_{ε} used in equations 21-23. The $We_{g,cr,0}$ value is also shown.

Breakup mode	$\boldsymbol{We_{g,cr,0}}$	$\boldsymbol{C_{vis,g}}$	$\boldsymbol{ng}$	$\boldsymbol{C_{vis,l}}$	$\boldsymbol{nl}$	$\boldsymbol{C_{\varepsilon}}$

bag	10	55	1.1	0.26	1.0	3
transitional	16	55	1.1	0.20	1.0	3
Sheet-thinning	63	55	1.1	0.06	1.0	3
catastrophic	350	55	1.1	0.01	1.0	3

233

234 A graphical representation of the aforementioned correction factors is shown in Fig.1,
235 according to which liquid viscosity effects become important for Ca_l>0.5, gas
236 viscosity effects for Re_g<300 and density ratio effects for ε<20.

237

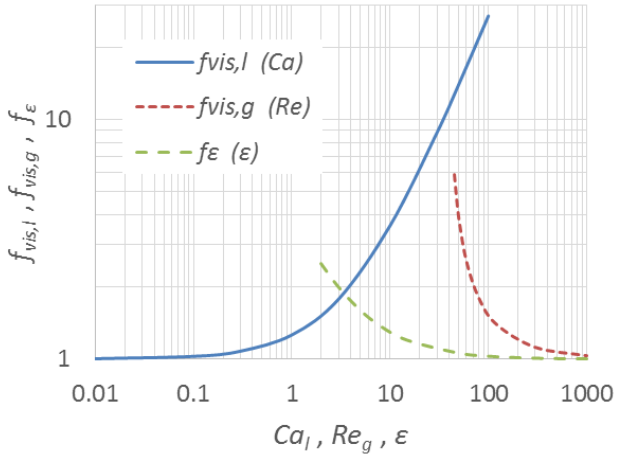

238

239 Fig.1: Correction factors for the effect of Ca_l (for bag breakup), Re_g and density ratio
240 ε.

241

242 A final comment has to be made as concerns the methodology described in this
243 section. It represents an extension of the experimental observations for the dominant

role that We_g number plays on distinguishing and controlling breakup regimes and it is not based on a physical principle, such as the momentum conservation equation or the deformation of the droplet beyond a threshold (e.g. the R-T wavelength). Nevertheless, in the appendix (section 6.3) it is proved that the model equations are equivalent to those obtained by using a modified version of the energy approach by (Cohen, 1994). As it will be shown in the following sections, the present model provides with sufficient accuracy a unified criterion to predict the breakup outcome for any combination of We_g, Ca_l (or Oh_l), Re_g and ε numbers.

3 Results and discussion

3.1 Qualitative model performance

In this section the qualitative model performance is examined by using equations 20-23 and adopting some reference values for the Re_g number and density ratio ε (equal to 1000 for both) to calculate the correction factors $f_{vis,g}$ and f_{ε}. Except of the classical $We_g - Oh_l$ breakup map, alternative breakup maps in the $We_g - Re_{l/g}$ and $We_g - Ca_l$ planes are also presented.

3.1.1 The $We_g - Oh_l$ plane

In order to reproduce the $We_g - Oh_l$ plane, the Ca_l number in eq. 23 is replaced with $Ca_l = Oh_l\sqrt{We_g}$ (see eq. 12). Using these modifications and setting *nl*=1, eq 20 is transformed into:

$$\frac{We_{g,cr}}{We_{g,cr,0}} = f_\varepsilon \cdot f_{vis,g} \cdot \left(1 + C_{vis,l}\sqrt{We_g} \cdot Oh_l\right) \tag{24}$$

This is a quadratic equation in respect to $\sqrt{We_g}$ having two roots. Keeping only the positive one, the final expression for the dependency of We_g versus Oh_l is given in equation 25.

$$We_{g,cr} = \frac{1}{4}\left[\left(C_{vis,l} \cdot We_{g,cr,0} \cdot f_\varepsilon \cdot f_{vis,g} \cdot Oh_l\right) + \sqrt{\left(C_{vis,l} \cdot We_{g,cr,0} \cdot f_\varepsilon \cdot f_{vis,g} \cdot Oh_l\right)^2 + 4We_{g,cr,0} \cdot f_\varepsilon \cdot f_{vis,g}}\right]^2 \tag{25}$$

The model results for the bag breakup mode ($We_{g,cr,0}$, =10) are shown in Fig.2 along with the corresponding correlations from similar referenced works. As it can be seen, the present model can capture the qualitative behaviour of the dependency between $We_{g,cr}$ and Oh_l, while it is very close to the results of (Hsiang and Faeth, 1995). Similar agreement has been achieved for the transitional and the sheet-thinning breakup regimes, using the adequate coefficients $C_{vis,l}$.

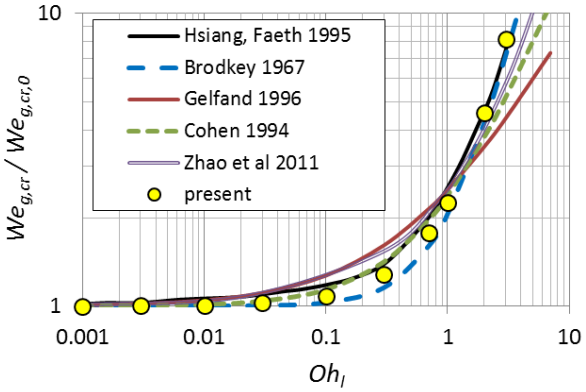

Fig.2: Results of the present model for the bag breakup regime in the We_g – Oh_l plane. The corresponding results from other correlations are also shown.

Regarding the effect of Re_g number and density ratio on the critical We_g number, this is shown in Fig.3 for the bag breakup case ($We_{g,cr,0}$=10), which is representative for all breakup modes. As seen, decreasing the Re_g and ε numbers results in a slight increase of the critical We_g number. This is in accordance with the findings of past works presented in the introduction.

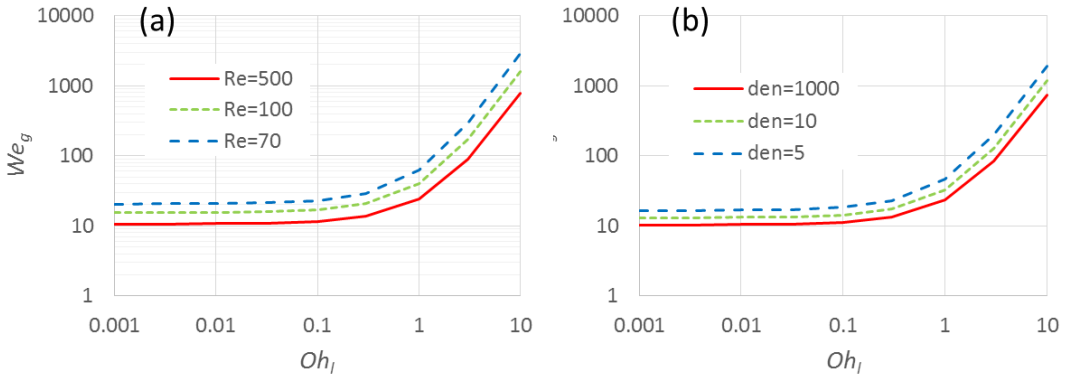

Fig.3: (a) effect of Re number, (b) effect of density ratio on the bag breakup boundary.

Regarding the asymptotic behavior of eq. 24 for large *Oh* numbers, the product $C_{vis,l}\sqrt{We_g}\cdot Oh_l$ is much higher than unity, thus equation 24 becomes $\sqrt{We_g}/Oh_l = f_\varepsilon \cdot f_{vis,g} \cdot C_{vis,l} \cdot We_{g,cr,0}$, which is a constant number. This is in accordance with the findings of (Aalburg, 2002) and (Zhao et al., 2011); the first one proved this by performing numerical simulations and the second one by using the R-T instabilities theory.

3.1.2 Alternative breakup planes

Alternative breakup planes can be developed by using directly eq. 23 (for the We_g – Ca_l plane) or by replacing the Ca_l number in eq. 23 with $Ca_l = We_g/Re_{g/l}$ (from eq. 12) in order to develop the We_g – $1/Re_{g/l}$ plane; after some manipulation, the resulting equation is eq. 26. As in the previous case, the coefficient *nl* in eq. 23 has been set equal to 1.

$$\frac{We_{g,cr}}{We_{g,cr,0}} = \frac{f_\varepsilon \cdot f_{vis,g}}{1 - f_\varepsilon \cdot f_{vis,g} \cdot C_{vis,l} \frac{1}{Re_{g/l}} We_{g,cr,0}} \tag{26}$$

The planes We_g – Ca_l and We_g – $1/Re_{g/l}$ are plotted in Fig.4a, b respectively by using the same coefficients as in section 3.1.1 for the We_g – Oh_l plane. All planes presented so far look similar to one another, but there is a substantial difference in the We_g – $1/Re_{g/l}$ plane. In this plane based on eq. 26 there is a critical condition for breakup, i.e $1/Re_{g/l} < 1/\left(f_\varepsilon \cdot f_{vis,g} \cdot C_{vis,l} \cdot We_{g,cr,0}\right)$. This means that breakup is not always observed for high $1/Re_{g/l}$ numbers. This contradicts the results deduced from the We_g – Oh_l and We_g – Ca_l planes in which there is no limitation for breakup. For the time being, there are no experimental data examining extremely high values of $\sqrt{We_g}/Oh_l$ (or We_g/Ca_l, or $1/Re_{g/l}$), thus a clear suggestion for the most appropriate breakup plane, cannot be given.

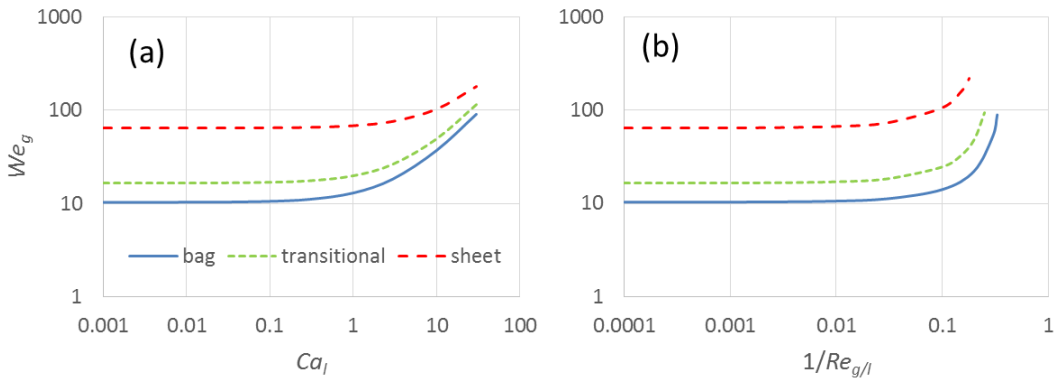

309

310 Fig.4: Results of the present model in (a) the We_g – Ca_l plane and (b) the We_g – $1/Re_{g/l}$
311 plane.

312

313 Among the breakup planes presented so far, our opinion is that the most suitable is the
314 We_g – Ca_l plane, since its axes represent gas inertia versus liquid viscous forces, both
315 non-dimensionalised with the same quantity, i.e the liquid surface tension forces,
316 while the asymptotic behavior at large We_g/Ca_l values agrees with the one predicted
317 by (Aalburg, 2002) and (Zhao et al., 2011). Furthermore, there is an explicit relation
318 between We_g and Ca_l for any value of the coefficient *nl*, while for the other numbers
319 (Oh_l or $Re_{g/l}$) there is an implicit relation with the We_g number when *nl* is not unity.
320 For the aforementioned reasons, the We_g – Ca_l plane is further used in this work.

321

322 ## 3.2 Comparison against experimental and numerical data

323 In this section, a large amount of experimental and numerical data are superimposed
324 in the proposed We_g – Ca_l plane to reveal the model capabilities compared to other
325 works. It is of importance to highlight that the Re_g number and the density ratio are

not predefined by assuming reference values as in section 3.1, but they are explicitly calculated. The results presented here have been grouped according to the breakup outcome into a) non-breakup, b) bag breakup, c) transitional, d) sheet-thinning and finally e) catastrophic regimes. The transitional breakup regime includes the intermediate regimes bag-stamen, dual-bag, multi-bag and plume-shear for reasons of simplicity and clearness. For reasons of distinctness and readability, the experimental data and the numerical data are discussed in separate sections. Prior to the presentation of the results, the concept of the effective We_g number, is introduced.

3.2.1 The effective *We* number

In order to avoid using multi-dimensional graphs (or 2-dimensional planes with parametric curves as in Fig.3) for the cases in which different Re_g numbers or density ratios are examined, equation 20 is rearranged and the We_g number is replaced with an effective We_g number ($We_{g,eff}$), which takes into consideration the secondary effects of Re_g number and density ratio on breakup outcomes. This is numerically represented in eq. 27:

$$\frac{We_{g,eff}}{We_{g,cr,0}} = 1 + C_{vis,l} \cdot (Ca_l)^{nl}, \qquad We_{g,eff} = \frac{We_g}{f_\varepsilon \cdot f_{vis,g}} \tag{27}$$

For example, in a case with We_g=13, Re_g=70 and a density ratio equal to 10, the effective We_g number is:

$$We_{g,eff} = \frac{\mathbf{13}}{(1 + 3/\mathbf{10}) \cdot (1 - 55 \cdot \mathbf{70}^{-1.1})^{-1}} = \frac{13}{1.33 * 2.04} = 4.79$$

and probably the droplet will not breakup, since it is much lower than $We_{g,cr,0}$=10. On the other hand, in a case with large Re_g and density ratio (e.g 8000 and 1000 respectively), $We_{g,eff}$ is equal to 12.93, close to the normal We_g number of 13. Therefore, it is better and more straightforward for droplet breakup characterization, the $We_{g,eff}$ instead of the We_g number to be used. In the appendix (section 6.2), the effective We_g number is also used to predict the breakup initiation time.

3.2.2 Comparison against experimental data

The experimental data used to assess the model performance are presented separately according to the experimental technique used, i.e the shock tube and the continuous air jet. For the shock tube experiments (denoted as ST), there are 46 experimental points obtained from the works of (Hanson et al., 1963), (Hirahara and Kawahashi, 1992), (Hsiang and Faeth, 1995), (Dai and Faeth, 2001), while for the continuous air jet experiments (CAJ), there are 101 experimental points obtained from the works of (Krzeczkowski, 1980),(Arcoumanis et al., 1994), (Liu and Reitz, 1997), (Lee and Reitz, 2000), (Zhao et al., 2010), (Opfer et al., 2012), (Flock et al., 2012), (Jain et al., 2015). The results of the present model are shown in Fig.5(a) and (b) for both the experimental techniques (ST and CAJ respectively).

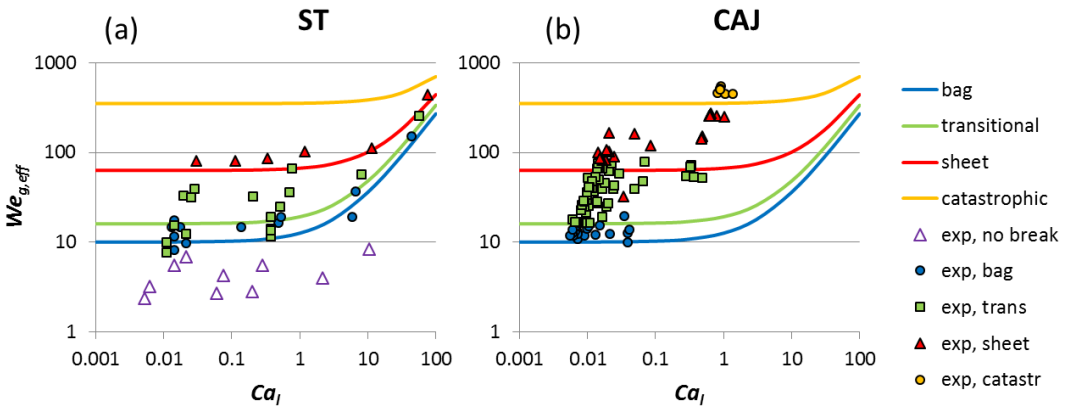

362

363 Fig.5: Results of the present model in the $We_{g,eff} - Ca_l$ plane for (a) Shock Tube and
364 (b) Continuous Air Jet experiments.

365

366 As seen, the fitting of the experimental data is generally good, especially for the CAJ
367 experiments with an exception for one experimental point of (Flock et al., 2012) in the
368 sheet-thinning regime, which was observed at a small We_g number of 32, rather
369 corresponding to the transitional regime; nevertheless, in the experimental photos of
370 this case, the sheet formation was clear. Also the experiments by Reitz and co-
371 workers (Liu and Reitz, 1997), (Lee and Reitz, 2000) at We_g=54 were considered as
372 "bag" in the relevant paper, but from their experimental photos it seems rather to
373 undergo a multi-bag breakup; thus in the present paper they were included in the
374 "transitional" regime. Regarding the ST experiments, there is a scattering in the
375 transitional breakup regime in which there are some cases (5 from (Hanson et al.,
376 1963) and 1 from (Hirahara and Kawahashi, 1992)) characterized by a relatively low
377 *We* number of 7-8 which exhibit bag-stamen breakup regime. Nevertheless, it is not
378 always clear what someone considers as bag or bag-stamen, while other parameters
379 such as the Mach number and turbulence levels may affect the breakup outcome. Such

secondary controlling physical parameters have not been considered in the present model.

In relevance to the breakup map of (Hsiang and Faeth, 1995), the boundary of transitional breakup appears for lower values of We_g number, and includes the bag-stamen, dual-bag, bag-plume, shear plume breakup regimes. The determination of this regime was mainly based on the experiments of (Zhao et al., 2010), which are more recent than the experiments of (Hsiang and Faeth, 1995). One should recall also, that these two works use a different experimental technique.

3.2.3 Comparison against numerical data

In this section the model performance is compared against numerical 2D axisymmetric simulations. The numerical data used to assess the model performance are 66 simulations performed in the past from the authors' group in (Strotos et al., 2016a, b; Strotos et al., 2016c), as well as simulations performed in the current work (see appendix), and 43 simulations from (Han and Tryggvason, 2001). For reasons of readability these are presented in different graphs, i.e. in Fig.6 (a) and (b) respectively. The "forward bag" observed in (Han and Tryggvason, 2001) was included in the transitional regime here. In these simulations the Re_g number was in the range 50 – 4000 and the density ratio in the range 5 – 800, which means that there are cases (those with low Re_g and ε) in which the effective $We_{g,eff}$ number differs significantly among them compared to using the classical We_g number. This is an additional reason, why the use of the effective We_g number is proposed as more

representative for such types of droplet breakup characterization, compared to the standard one.

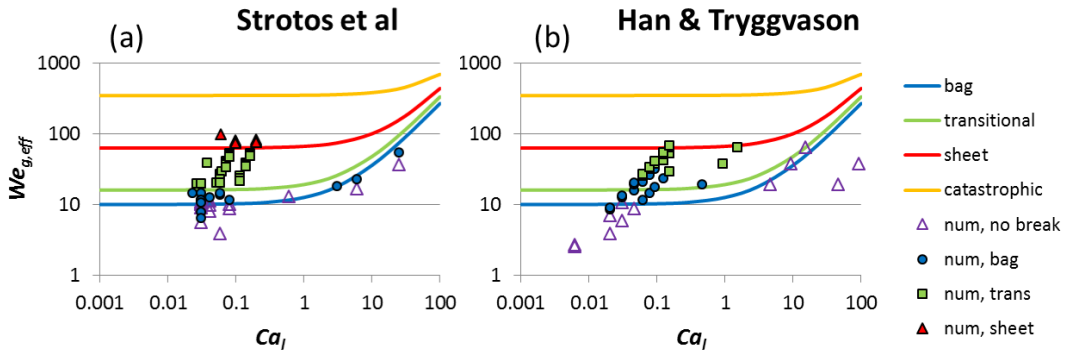

Fig.6: Results of the present model in the $We_{g,eff} - Ca_l$ plane for (a) simulations of the authors' group and (b) simulations of (Han and Tryggvason, 2001).

Based on the graphs, the overall model performance towards separating the various breakup regimes is good and only a few exceptions seem to deviate from the proposed breakup boundaries. In the authors' group simulations, there are two cases which breakup but appear in the non-breakup region of the map, whilst in the (Han and Tryggvason, 2001) simulations, there are 5 bag breakup cases which appear in the transitional region of the map. Nevertheless, in all these cases (characterized by low Re_g numbers and density ratios) the breakup modes differ from those observed in the experiments and it is a matter of convention what someone considers as transitional breakup. Furthermore, the breakup phenomenon is a continuous process (as stated in (Guildenbecher et al., 2009)) and there is not yet a deterministic single criterion for the transition among different breakup regimes. Based on their recommendation a zone rather than a single line should be used to separate the breakup regimes.

However, the present work offers the introduction of an alternative set of parameters for visualizing the transition of droplet breakup mechanisms, which seems to be more representative and close to reality compared to previous work and in that respect should be considered as a step-forward towards understanding the underling physics represented by more correct variables.

4 Conclusions

In the present work, a new proposed total force approach has been used to determine the dependency of the critical We_g number ($We_{g,cr}$) separating different breakup regimes on all other non-dimensional numbers (Re_g, ε and Oh_l or Ca_l). According to this approach, the breakup phenomenon is controlled by the ratio of the sum of the deformation versus the sum of restorative forces; for negligible viscosities, this ratio reduces to the classical We_g number. Breakup (or generally transition between breakup regimes) occurs when this ratio exceeds a critical value; the latter is equal to the critical We_g number corresponding to low Oh_l numbers (termed here as $We_{g,cr,0}$) and it is known from experimental data.

The proposed model includes adjustable coefficients, which were determined by performing numerical simulations and comparing against a large amount of experimental and numerical data found in literature. Overall, a good qualitative and quantitative agreement has been achieved. To unify cases with different conditions (namely Re_g and ε numbers) an effective We_g number ($We_{g,eff}$) was proposed. This is essentially the classical We_g number, corrected by two factors which account for the secondary effects of Re_g and ε numbers. The model results were presented in a new

breakup map, the $We_{g.eff} - Ca_l$ plane; using the Ca_l number instead of the Oh_l, corresponds directly to the relation of gas inertia versus liquid viscosity when both are non-dimensionalised using the same quantity (the surface tension forces), while using the $We_{g,eff}$ instead of the We_g number, enables the inclusion of additional parameters in the same plane. The effective $We_{g,eff}$ number was also used to predict the breakup initiation time, shown in the appendix

The present methodology is not derived from physical principles, such as the momentum equation or the Rayleigh-Taylor instabilities. It is rather an extension of experimental observations and numerical data towards including in a unified way all possible interdependencies among the forces acting on a droplet. Nevertheless, it is shown in the appendix that this model is fully compatible with an energy approach relating the required kinetic energy for breakup with that of an inviscid droplet. The methodology proposed applies for Newtonian fluids, in laminar, isothermal and incompressible flow conditions.

5 Acknowledgement

The authors would like to acknowledge the support of the ERSRC project No EP/K02052028/1

6 Appendix

6.1 Derivation of correction factors

In this section, the 2D axisymmetric simulations performed for the determination of the correction factors $f_{vis,g}$ and f_{ε} are presented. To determine these factors, all parameters were kept constant and only one was changing each time to reveal the effect of Re_g number and density ratio; the reference settings used were Ca_l=0.03, Re_g=400 and ε=800. The cases examined were 55 and 31 of them are presented in detail in Table 3. The VOF methodology (Hirt and Nichols, 1981) has been used and implemented in ANSYS FLUENT v16.1 (ANSYS®FLUENT, 2015); details on the methodology used can be found in earlier authors' work mentioned in section 3.2.3. Note also that here, only the breakup outcome is presented, grouped into "breakup", "no breakup" and "marginal", with the latter representing cases with an unclear breakup outcome; more details on the droplet shapes and physical mechanisms are going to be published in a separate article.

Table 3: List of the physical parameters of selected cases for the determination of the correction factors.

We_g	Re_g	Oh_l	Ca_l	ε	N
25	50.0	0.006	0.03	800	1.70
30	50.0	0.005	0.03	800	1.41
30	70.0	0.005	0.03	800	1.98
14	100.0	0.008	0.03	800	6.06
16	100.0	0.008	0.03	800	5.30
20	100.0	0.007	0.03	800	4.24
30	100.0	0.005	0.03	800	2.83
12	200.0	0.009	0.03	800	14.14

We_g	Re_g	Oh_l	Ca_l	ε	N
13	200.0	0.008	0.03	800	13.05
14	200.0	0.008	0.03	800	12.12
11	400.0	0.009	0.03	800	30.86
11	400.0	0.009	0.03	800	30.86
11	400.0	0.009	0.03	800	30.86
12	400.0	0.009	0.03	800	28.28
12	400.0	0.009	0.03	800	28.28
12	400.0	0.009	0.03	800	28.28
11	2400.0	0.009	0.03	800	185.13
12	400.0	0.009	0.03	100	10.00
13	400.0	0.008	0.03	20	4.13
14	400.0	0.008	0.03	20	3.83
16	400.0	0.008	0.03	10	2.37
16	400.0	0.008	0.03	5	1.68
20	400.0	0.007	0.03	5	1.34
20	400.0	0.007	0.03	3	1.04
20	400.0	0.007	0.03	2	0.85
14	400.0	0.160	0.6	800	484.87
20	400.0	0.671	3	800	1697.06
18	400.0	1.414	6	800	3771.24
25	400.0	1.200	6	800	2715.29
40	400.0	3.953	25	800	7071.07
60	400.0	3.227	25	800	4714.05

6.1.1 Effect of gas viscosity

The effect of gas viscosity (i.e the Re_g number) on droplet breakup for Ca_l=0.03, ε=800 is presented in Fig.7 in a We_g – Re_g plane. The curve representing the limiting condition for breakup is $11.1\cdot(1-55\cdot Re^{-1.1})^{-1}$, while the corresponding curve representing the data of (Han and Tryggvason, 2001) for ε=10 is also shown. As seen, the present results are in qualitative agreement with those of (Han and Tryggvason, 2001) despite the fact that the density ratios are different; additional simulations are required to investigate possible dependency on the density ratio and the Ca_l (or Oh_l) number.

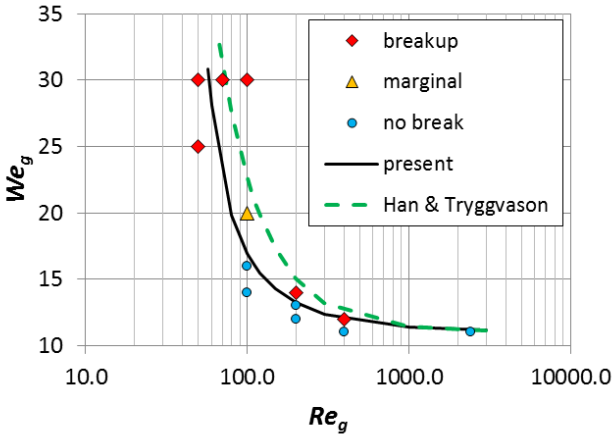

Fig.7: Effect of gas viscosity (Re_g number) on droplet breakup for Ca_l=0.03, ε=800. A curve representing the corresponding results of (Han and Tryggvason, 2001) for ε=10, is also shown.

6.1.2 Effect of density ratio

The effect of density ratio on droplet breakup for Ca_l=0.03, Reg=400 is shown in Fig.8 in a $We_g - \varepsilon$ plane. The curve representing the limiting condition for breakup is 11.5(1+3·1/ε) and it is in close agreement with the one representing the data of (Aalburg, 2002) for Re_g=50 and Oh_l=0.001 in which the correction factor was estimated (by the authors of the present work) to be exp(2.68/ε); possible dependency on the Ca_l (or the Oh_l) number was not examined and additional simulations are required for that. A final comment has to be made for the correction factor $f\varepsilon$=1+C_ε·1/ε used to account for the effect of density ratio. Since the density ratio ε is not appearing in the TFR number, it was "manually" included in the present analysis. Nevertheless, its form is not arbitrary. It was inspired by the work of (Jalaal and Mehravaran, 2014) who found that the interfacial instabilities on the droplet's surface begin at a We_g number which is analogous to (1+ 1/ε).

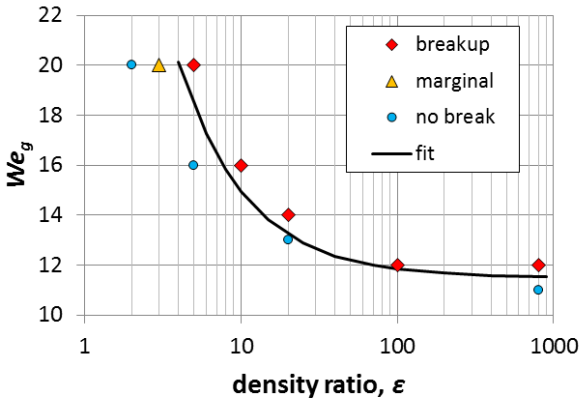

507

508 Fig.8: Effect of density ratio on droplet breakup for Ca_l=0.03, Re=400.

509

510 6.2 Estimation of the breakup initiation time

511 The effective We_g number ($We_{g,eff}$) defined in section 3.2.1 can be used to include the
512 effects of Re_g number and density ratio on the breakup initiation time. Generally,
513 there is not a clear definition what is meant by the term "initiation" time. Here,
514 breakup initiation time is the instant at which there is droplet detachment or the
515 instant at which the droplet interface is corrupted and holes are created. Analyzing the
516 numerical data used in section 3.2.3, the following equation 28 can be used to predict
517 the breakup initiation time, with less than 20% error (see Fig.9):

$$\frac{t_{break}}{t_{sh}} = 2.87\left(We_{g,eff} - 8\right)^{-0.26}\left(1 + 2.56Oh_l^{0.63}\right) \tag{28}$$

518 This equation has the same form as the one proposed by (Pilch and Erdman, 1987),
519 but additionally predicts that the breakup time increases with decreasing Re_g and ε
520 numbers. In (Pilch and Erdman, 1987) the dependency of break initiation time versus
521 the We_g number was analogous to $(We_g - 12)^{-0.25}$ and in (Reinecke and Waldman,

1975) proportional to $(We_g - 8)^{-0.25}$. Here an exponent of –0.26 has been estimated, which is close to the aforementioned values.

Regarding the overall behavior of eq. 28 in relevance to other correlations based on experimental data, the predicted breakup time is in-between the one predicted by the correlations of (Pilch and Erdman, 1987) and (Dai and Faeth, 2001) for a wide range of We_g numbers (all others parameters regarded constant), while it predicts a similar effect of Oh_l number as the one predicted by the correlations of (Pilch and Erdman, 1987),(Hsiang and Faeth, 1992),(Gelfand, 1996). These trends are shown in Fig.10.

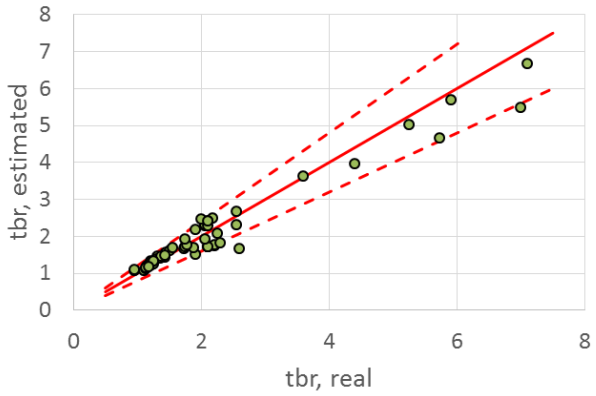

Fig.9: Prediction of breakup initiation time with eq. 28. The error lines of ±20% are also shown.

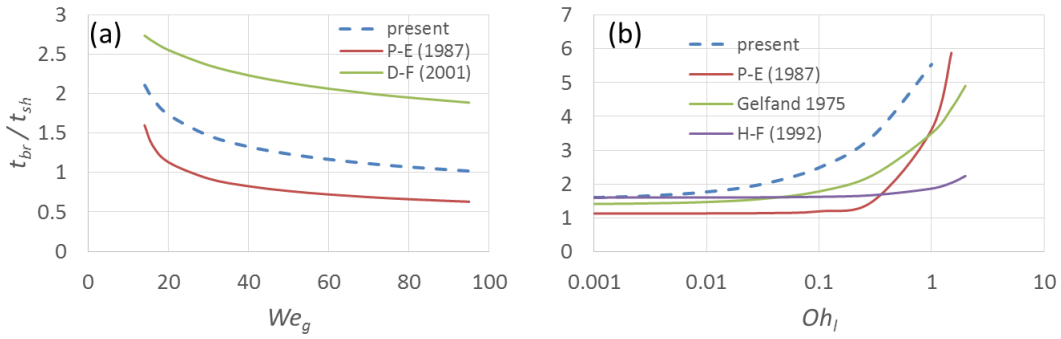

Fig.10: Prediction of breakup initiation time with eq. 28. (a) effect of We_g, (b) effect of Oh_l number. Correlations from other researchers are also shown.

6.3 Relation to Cohen's approach

In (Cohen, 1994) it was assumed that the kinetic energy required for breakup is that of an inviscid droplet plus the energy required to overcome the energy dissipated by the liquid viscosity; this is shown mathematically in eq. 29 including also the dissipation in the gas phase.

$$\frac{1}{2}\frac{\pi D^3}{6}\rho_g U_g^2 = \left(\frac{1}{2}\frac{\pi D^3}{6}\rho_g U_g^2\right)_{vis=0} + C_{vis,l}(\mu_l U_l D^2) + C_{vis,g}\left(\mu_g U_g D^2\right) \tag{29}$$

In relevance to Cohen's approach, in the liquid dissipation term he assumed that there is a "mixing velocity" U_{mix}, which was determined by comparing against experimental data; instead of that here, the liquid phase velocity U_l is used, along with the adjustable coefficient $C_{vis,l}$. Non-dimensionalising eq 29 with the surface energy of the spherical droplet $\sigma\pi D^2$, and substituting the liquid velocity from eq. 4, we get equation 30 in which the We_g number in the limit of inviscid flow ($We_{g,cr,0}$) has appeared in the RHS of the equation.

$$We_g = We_{g,cr,0} + 12\frac{C_{vis,l}}{\pi}Ca_l + 12\frac{C_{vis,g}}{\pi}\frac{We_g}{Re_g} \tag{30}$$

Rearranging eq. 30 and dividing by $We_{g,cr,0}$ we get eq. 31 which is identical to the equation derived with the total force approach in section 2.2 (with ng, nl, $f\varepsilon$ equal to unity and including all constants inside the terms $C_{vis,g}$ and $C_{vis,l}$)

$$\frac{We_g}{We_{g,cr,0}}\left(1-\left(12\frac{C_{vis,g}}{\pi}\right)\frac{1}{Re_g}\right)=1+\left(12\frac{C_{vis,l}}{\pi We_{g,cr,0}}\right)Ca_l \quad (31)$$

7 Nomenclature

Roman symbols

Symbol	Description	Units
C	Adjustable coefficient	-
Ca	Capillary number $Ca = \mu U/\sigma$	-
D	diameter	m
f	Correction factor	-
F	force	N
n,ng,nl	Adjustable exponent	
Oh	Ohnesorge number $Oh = \mu/\sqrt{\rho\sigma D}$	-
Re	Reynolds number $Re = \rho UD/\mu$	-
t	time	s
U	reference velocity	m/s
We	Weber number $We = \rho U^2 D/\sigma$	-

Greek symbols

Symbol	Description	Units
ε	density ratio $\varepsilon = \rho_l/\rho_g$	-
μ	viscosity	kg/ms
N	Viscosity ratio $N = \mu_l/\mu_g$	
ρ	density	kg/m^3
σ	surface tension coefficient	N/m

Subscripts

Symbol	Description
0	Reference value
br	breakup
cr	critical
DEF	deformation
eff	effective
g or gas	gas
l or liq	liquid
RES	restore
vis	viscosity

Abbreviations

Symbol	Description
CAJ	Continuous Air Jet
R-T	Rayleigh-Taylor
ST	Shock tube
TFR	Total Force Ratio
VOF	Volume of Fluid

8 References

Aalburg, C., 2002. Deformation and breakup of round drop and nonturbulent liquid jets in uniform crossflows, Aerospace Engineering and Scientic Computing. University of Michigan.

ANSYS®FLUENT, 2015. Release 16.1, Theory Guide.

Arcoumanis, C., Khezzar, L., Whitelaw, D.S., Warren, B.C.H., 1994. Breakup of Newtonian and non-Newtonian fluids in air jets. Experiments in Fluids 17, 405-414.

Brodkey, R.S., 1967. Formation of drops and bubbles, The phenomena of fluid motions. Addison-Wesley, Reading, Mass.

Cohen, R.D., 1994. Effect of viscosity on drop breakup. International Journal of Multiphase Flow 20, 211-216.

Dai, Z., Faeth, G.M., 2001. Temporal properties of secondary drop breakup in the multimode breakup regime. International Journal of Multiphase Flow 27, 217-236.

Flock, A.K., Guildenbecher, D.R., Chen, J., Sojka, P.E., Bauer, H.J., 2012. Experimental statistics of droplet trajectory and air flow during aerodynamic fragmentation of liquid drops. International Journal of Multiphase Flow 47, 37-49.

Gelfand, B.E., 1996. Droplet breakup phenomena in flows with velocity lag. Progress in Energy and Combustion Science 22, 201-265.

Guildenbecher, D.R., López-Rivera, C., Sojka, P.E., 2009. Secondary atomization. Experiments in Fluids 46, 371-402.

Han, J., Tryggvason, G., 2001. Secondary breakup of axisymmetric liquid drops. II. Impulsive acceleration. Physics of Fluids 13, 1554-1565.

582 Hanson, A.R., Domich, E.G., Adams, H.S., 1963. Shock Tube Investigation of the Breakup of
583 Drops by Air Blasts. The Physics of Fluids 6, 1070-1080.

584 Hinze, J.O., 1949. Critical speeds and sizes of liquid globules. Flow, Turbulence and
585 Combustion 1, 273.

586 Hinze, J.O., 1955. Fundamentals of the hydrodynamic mechanism of splitting in dispersion
587 processes. AIChE Journal 1, 289-295.

588 Hirahara, H., Kawahashi, M., 1992. Experimental investigation of viscous effects upon a
589 breakup of droplets in high-speed air flow. Experiments in Fluids 13, 423-428.

590 Hirt, C.W., Nichols, B.D., 1981. Volume of Fluid (Vof) Method for the Dynamics of Free
591 Boundaries. Journal of Computational Physics 39, 201-225.

592 Hsiang, L.P., Faeth, G.M., 1992. Near-limit drop deformation and secondary breakup.
593 International Journal of Multiphase Flow 18, 635-652.

594 Hsiang, L.P., Faeth, G.M., 1995. Drop deformation and breakup due to shock wave and
595 steady disturbances. International Journal of Multiphase Flow 21, 545-560.

596 Jain, M., Prakash, R.S., Tomar, G., Ravikrishna, R.V., 2015. Secondary breakup of a drop at
597 moderate Weber numbers. Proceedings of the Royal Society of London A: Mathematical,
598 Physical and Engineering Sciences 471.

599 Jalaal, M., Mehravaran, K., 2014. Transient growth of droplet instabilities in a stream.
600 Physics of Fluids 26, 012101.

601 Jing, L., Xu, X., 2010. Direct Numerical Simulation of Secondary Breakup of Liquid Drops.
602 Chinese Journal of Aeronautics 23, 153-161.

603 Joseph, D.D., Belanger, J., Beavers, G.S., 1999. Breakup of a liquid drop suddenly exposed to
604 a high-speed airstream. International Journal of Multiphase Flow 25, 1263-1303.

605 Kékesi, T., Amberg, G., Prahl Wittberg, L., 2014. Drop deformation and breakup.
606 International Journal of Multiphase Flow 66, 1-10.

607 Krzeczkowski, S.A., 1980. Measurement of liquid droplet disintegration mechanisms.
608 International Journal of Multiphase Flow 6, 227-239.

Lee, C.H., Reitz, R.D., 2000. An experimental study of the effect of gas density on the distortion and breakup mechanism of drops in high speed gas stream. International Journal of Multiphase Flow 26, 229-244.

Liu, Z., Reitz, R.D., 1997. An analysis of the distortion and breakup mechanisms of high speed liquid drops. International Journal of Multiphase Flow 23, 631-650.

Nicholls, J.A., Ranger, A.A., 1969. Aerodynamic shattering of liquid drops. AIAA Journal 7, 285-290.

Opfer, L., Roisman, I.V., Tropea, C., 2012. Aerodynamic Fragmentation of Drops: Dynamics of the Liquid Bag, ICLASS 2012, Heidelberg, Germany.

Pilch, M., Erdman, C., 1987. Use of breakup time data and velocity history data to predict the maximum size of stable fragments for acceleration-induced breakup of a liquid drop. International Journal of Multiphase Flow 13, 741-757.

Reinecke, W., Waldman, G., 1975. Shock layer shattering of cloud drops in reentry flight, 13th Aerospace Sciences Meeting. American Institute of Aeronautics and Astronautics.

Schmehl, R., 2002. Advanced modeling of droplet deformation and breakup for CFD analysis of mixture preparation, ILASS-Europe, Zaragoza.

Strotos, G., Malgarinos, I., Nikolopoulos, N., Gavaises, M., 2016a. Aerodynamic breakup of an n-decane droplet in a high temperature gas environment. Fuel 185, 370-380.

Strotos, G., Malgarinos, I., Nikolopoulos, N., Gavaises, M., 2016b. Numerical investigation of aerodynamic droplet breakup in a high temperature gas environment. Fuel 181, 450-462.

Strotos, G., Malgarinos, I., Nikolopoulos, N., Gavaises, M., 2016c. Predicting droplet deformation and breakup for moderate Weber numbers. International Journal of Multiphase Flow 85, 96–109.

Theofanous, T.G., Li, G.J., 2008. On the physics of aerobreakup. Physics of Fluids 20, 052103.

Theofanous, T.G., Mitkin, V.V., Ng, C.L., Chang, C.-H., Deng, X., Sushchikh, S., 2012. The physics of aerobreakup. II. Viscous liquids. Physics of Fluids 24, 022104.

636 Yang, W., Jia, M., Che, Z., Sun, K., Wang, T., 2017. Transitions of deformation to bag
637 breakup and bag to bag-stamen breakup for droplets subjected to a continuous gas flow.
638 International Journal of Heat and Mass Transfer 111, 884-894.

639 Yang, W., Jia, M., Sun, K., Wang, T., 2016. Influence of density ratio on the secondary
640 atomization of liquid droplets under highly unstable conditions. Fuel 174, 25-35.

641 Zhao, H., Liu, H.-F., Cao, X.-K., Li, W.-F., Xu, J.-L., 2011. Breakup characteristics of liquid
642 drops in bag regime by a continuous and uniform air jet flow. International Journal of
643 Multiphase Flow 37, 530-534.

644 Zhao, H., Liu, H.-F., Li, W.-F., Xu, J.-L., 2010. Morphological classification of low viscosity
645 drop bag breakup in a continuous air jet stream. Physics of Fluids 22, 114103.

646